PROCEEDINGS, Thirty-Fifth Workshop on Geothermal Reservoir Engineering
Stanford University, Stanford, California, February 1-3, 2010
SGP-TR-188

NUMERICAL MODELING OF SECONDARY THERMAL FRACTURES IN HOT DRY GEOTHERMAL RESERVOIRS

Xiaoxian Zhou[1], Atilla Aydin[1], Fushen Liu[2], David D. Pollard[1]

[1]Department of Geological and Environmental Sciences, Stanford University, Stanford, CA 94305
[2]Department of Civil and Environmental Engineering, Stanford University, Stanford, CA 94305
e-mail: xzhou1@stanford.edu

ABSTRACT

Fluid circulation through geothermal reservoirs may potentially induce large tensile thermal stresses at the large hydraulic fracture surface thereby produce secondary thermal fractures. These secondary thermal fractures could penetrate deeply into the reservoirs, the fluids may flow into regions of hotter rock, and thus the performance of geothermal reservoirs can be significantly enhanced. In this study, we used an integral equation method to calculate the thermal stresses in a reservoir due to the cooling of the main hydraulic fracture surface. Then the thermal stresses are used in the displacement discontinuity method to analyze the stability and propagation of the secondary thermal fractures. It is found that under the conditions of large temperature differences between the main hydraulic fracture and the initial reservoir temperature, and relatively small in-situ stresses, the secondary thermal fractures could propagate deeply into the reservoirs. The analysis of the secondary thermal fracture interaction reveals that faster cooling rate which is equivalent to the fluid injection rate in geothermal operations results in smaller secondary thermal fracture spacing.

INTRODUCTION

The hot dry rock (HDR) geothermal reservoir involves drilling two or more wells to suitable depths to connect permeable fractures of natural or man-made origin, injecting cold water into one well, and recovering hot water from the others (Hayashi et al., 1995). However, the HDR system cannot rely solely on conduction in the rock for the thermal energy extraction. The thermal diffusivity of rock is relatively low (typically 10^{-6} m^2/sec for granite), which leads to the fact that the thermal front only can penetrate about 50m from the main hydraulic fracture into the reservoir even after 20 years of fluid circulation. The temperature of much of the fracture surface is expected to approach that of the injected cold water after several months of operation. Once this occurs, the power output of the HDR system will be at a rather low level.

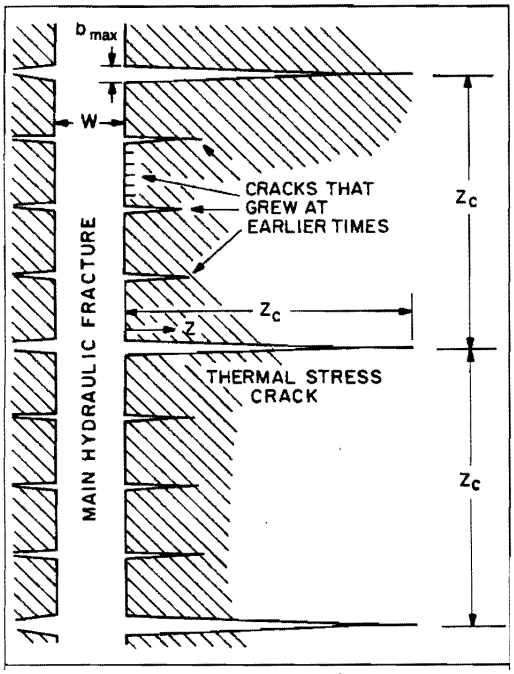

Figure 1. Idealized patterns of secondary thermal fractures (after Tester et al., 1989).

In the process of the cold water injection into the main hydraulic fracture, it has been found that the thermal stress components which are parallel to the fracture surface are much larger in magnitude than its component normal to the fractures surface (Zhou et al., 2009). Such a large parallel component of the thermal stresses may potentially create secondary thermal fractures in the geothermal reservoirs (see Figure 1). If the secondary thermal fractures could propagate deeply into the geothermal reservoir, the contact between injected water and the hot reservoir would increase, thus the productivity of the HDR system would be enhanced significantly.

Until now there are only a few publications on the secondary thermal fracture, such as Hsu (1978), Barr (1980) and Tester (1989). However, most of the work was based on unrealistic assumptions, such as constant propagation velocity of secondary thermal

fractures, closed secondary thermal fractures, no interaction of secondary thermal fractures, etc. In this paper, we will investigate the initiation, propagation, and interaction of the secondary thermal fractures by using numerical methods. The thermal loading is simulated by directly assuming a lower uniform temperature on the main hydraulic fracture compared to the reservoir temperature. We use a boundary integral equation method (Cheng et al., 2001; Zhou et al., 2009) to calculate the thermal stresses, which are then incorporated into the displacement discontinuity method (Crouch and Starfield, 1983) to analyze the secondary thermal fracture problem.

THERMOELASTIC MODEL

The field equations and constitutive model for the thermoelasticity in solid mechanics are briefly described as follows. The constitutive equation for the stress-strain relation and the heat transport equation can be written as (Jaeger *et al*., 2007)

$$\boldsymbol{\sigma} = 2G\boldsymbol{\varepsilon} + \left(K - \frac{2G}{3} \right) \text{trace}(\boldsymbol{\varepsilon}) \mathbf{I} + 3\beta K T \mathbf{I} \tag{1}$$

$$\mathbf{q}_T = -\mathbf{k}_T \nabla T \tag{2}$$

where $\boldsymbol{\sigma}$ and $\boldsymbol{\varepsilon}$ are respectively the stress and strain tensors, K and G are respectively bulk modulus and shear modulus of material, T is the temperature, β is the coefficient of linear thermal expansion, $\mathbf{q}_T$ is the conductive heat-flux vector, $\mathbf{k}_T$ is the thermal conductivity tensor, and $\mathbf{I}$ is the unit matrix.

The above constitutive equations and transport equations can be combined with the momentum and energy balance equations, to yield the following field equations:

$$G\nabla^2 \mathbf{d} + \left(K + \frac{G}{3} \right) \nabla \left(\nabla \cdot \mathbf{d} \right) = -\mathbf{f} - 3\beta K \nabla T \tag{3}$$

$$\dot{T} - c^T \nabla^2 T = 0 \tag{4}$$

where $\mathbf{d}$ is the displacement vector, and $\mathbf{f}$ is the body-force vector per unit volume. Eqs. (3) and (4) can be used together with mechanical and heat transfer boundary and initial conditions to solve thermoelastic problems.

NUMERICAL MODEL

Integral Equation Solution for Thermal Stresses

In this study, it is assumed that the surface of the main hydraulic fracture is cooled suddenly and then maintained at a temperature T_f which is lower than the initial reservoir temperature T_r. The associated thermal stresses in this cooling process are solved using an integral equation technique (Zhou et al., 2009) in the time domain.

The heat source at the fracture surface can induce the variations of temperature and stresses in the reservoir matrix. The reaction of the reservoir is governed by the thermal-elastic mechanics. In two-dimensional problems, for any distribution of the heat source intensity $q_h(x', y', t')$ along a fracture l, the resultant temperature in the reservoir at location (x, y) and time t is given by

$$T(x, y, t) = \int_0^t \int_l q_h(x', y', t') T^{hi}(x - x', y - y', t - t') \, dl dt' + T_0 \tag{5}$$

where T_0 is the initial temperature in the reservoir. The thermally induced stresses in the reservoir matrix can also be calculated using $q_h(x', y', t')$ at the fracture surface:

$$\sigma_{ij}^h(x, y, t) = \int_0^t \int_l q_h(x', y', t') \sigma_{ij}^{hi}(x - x', y - y', t - t') \, dl dt' \tag{6}$$

In Eqs. (5) and (6), $T^{hi}(x - x', y - y', t - t')$ and $\sigma_{ij}^{hi}(x - x', y - y', t - t')$ are the fundamental solutions for the temperature and stresses at the location (x, y) and time t due to an instantaneous unit point heat source at location (x', y') and time t'. These fundamental solutions could be found in Banerjee (1994). In the present problem, Eq. (5) is applied directly to the fracture to solve the distribution of q_h as the temperature of the fracture surface is given in this work. Thereafter, Eq. (6) is used to calculate the thermal stresses in the reservoir as well as at the fracture surface. The discretizations of Eqs. (5) and (6) are similar to those in Zhou et al. (2009) for three-dimensional problems and not presented here.

Fracture Propagation Simulation

In this work, we assume that the rock is isotropic, homogeneous and linear-elastic, and thus the linear elastic fracture mechanics can be used to simulate the fracture behavior. The displacement discontinuity method (DDM) (Crouch and Starfield, 1983) is used for the mechanical analysis. The discretized form of DDM can be expressed as

$$\begin{aligned} \sigma_n^i &= \sum_{j=1}^N C_{ns}^{ij} D_s^j + \sum_{j=1}^N C_{nn}^{ij} D_n^j \\ \sigma_s^i &= \sum_{j=1}^N C_{ss}^{ij} D_s^j + \sum_{j=1}^N C_{sn}^{ij} D_n^j \end{aligned} \tag{7}$$

where C_{ns}^{ij}, C_{nn}^{ij}, C_{ss}^{ij}, and C_{sn}^{ij} are the plane-strain, elastic influence coefficients given in Crouch and Starfield (1983), D_s^j and D_n^j are displacement discontinuities in the shear and normal directions, and σ_s^i and σ_n^i are the shear and normal stresses at the fracture surfaces. In this study, we let

$$\begin{aligned} \sigma_n^i &= \sigma_n^{remote} + \sigma_n^h \\ \sigma_s^i &= \sigma_s^{remote} + \sigma_s^h \end{aligned} \tag{8}$$

where σ_n^{remote} and σ_s^{remote} are the resolutions of the remote boundary stresses acting perpendicular and parallel to the elements, and σ_n^h and σ_s^h are the resolutions of the thermally induced stresses acting perpendicular and parallel to the elements. σ_n^h and σ_s^h can be calculated from σ_{ij}^h in Eq. (6) through coordinate transformation.

As given by Olson (1991), the stress intensity factor (SIF) can be computed as a function of the displacement discontinuities at the crack tip element i:

$$\begin{aligned} K_I &= 0.806\left(\frac{\sqrt{\pi}E}{4\left(1-\nu^2\right)\sqrt{2a}}\right)D_n^i \\ K_{II} &= 0.806\left(\frac{\sqrt{\pi}E}{4\left(1-\nu^2\right)\sqrt{2a}}\right)D_s^i \end{aligned} \tag{9}$$

where E is the Young's moduli, ν is the Poisson's ratio, and a is the half length of the tip element.

The equivalent SIF based on the maximum circumferential stress theory (Erdogan and Sih, 1963) is used here:

$$K_{eq} = \cos\frac{\theta_0}{2}\left(K_I\cos^2\frac{\theta_0}{2} - \frac{3}{2}K_{II}\sin\theta_0\right) \tag{10}$$

where θ_0 can be determined by solving the following equation:

$$K_I\sin\theta_0 + K_{II}\left(3\cos\theta_0 - 1\right) = 0 \tag{11}$$

The fracture propagation takes place when K_{eq} exceeds the material fracture toughness K_{IC}.

Recently, Mutlu and Pollard (2008) combined the DDM with a complementarity algorithm to model the quasi-static formation and patterns of wing crack along a sliding fault surface. We adopted their method in this work to improve the efficiency and accuracy of the fracture propagation simulation.

DISTRIBUTION AND EVOLUTION OF THERMAL STRESSES

In this work, we did not simulate the fluid flow in the fractures and the heat exchange between the cold water and hot reservoir. Instead, the surface of the main hydraulic fracture is suddenly cooled and then maintained at a lower temperature than the geothermal reservoir. To investigate the initiation and propagation of the secondary thermal fractures, first we will analyze the thermally induced stress distributions and evolutions in the geothermal reservoir using the integral equation method, namely Eqs. (5) and (6).

Table 1. Parameters and data set used in the analysis

Parameters	Values
Young's modulus E (GPa)	5
Poisson's ratio ν	0.25
Rock density ρ_r (kg/m^3)	2350
Rock heat capacity c_r (J/kg K)	600
Rock thermal conductivity K_r (W/m)	6
Rock linear thermal expansion coefficient α_T (1/K)	8×10^{-6}
Rock toughness K_{IC} (MPa m$^{1/2}$)	3.0
Fracture interface cohesion	0
Fracture interface friction	0
Maximum horizontal in-situ stress σ_{xx}^r (MPa)	50
Minimum horizontal in-situ stress σ_{yy}^r (MPa)	40
Reservoir temperature (K)	500
Fracture surface temperature (K)	300

In the numerical simulation, we assume the main hydraulic fracture is l=500 m and we calculate the thermal stresses along its perpendicular bisector. We assume that the temperature at the main fracture surface is maintained at 300 K, and the initial reservoir rock temperature is 500 K. The parameters used in the analysis can be found in Table 1. In this paper, *x* axis is along the main fracture and *y* axis is perpendicular to the main fracture.

Figure 2 shows the evolution of the thermally induced normal stresses σ_{xx}^h and σ_{yy}^h at the surface of the main hydraulic fracture, where σ_{xx}^h is the

component parallel to the fracture surface while σ_{yy}^{h} is the component normal to the fracture surface. σ_{xx}^{h} and σ_{yy}^{h} are respectively responsible to the opening of the main fracture and the initiation of the secondary thermal fractures. It is found that both σ_{xx}^{h} and σ_{yy}^{h} are tensile. σ_{yy}^{h} increases very slowly from zero at the beginning to around 40 MPa at 10^{10} sec, which indicates that in geothermal reservoirs, the opening of the main fracture due to the thermal stresses is only significant after a long term operations. However, σ_{xx}^{h} reaches its maximum value of about 100 MPa at the very beginning and then slowly decreases to 70 MPa at the time of 10^{10} sec. Such a large magnitude of σ_{xx}^{h} at the main fracture surface is sufficient to produce incipient secondary thermal fractures.

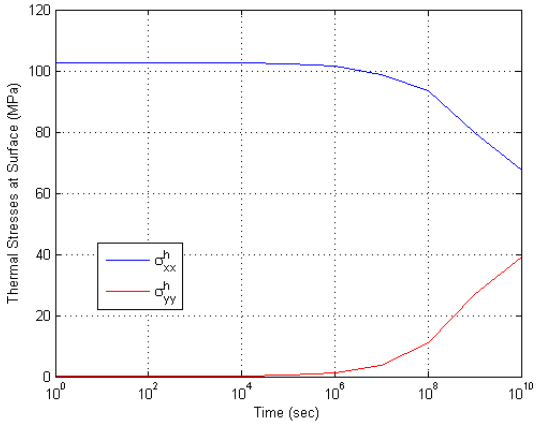

Figure 2. Evolution of thermally induced stresses at the surface of the main hydraulic fracture, where σ_{xx}^{h} and σ_{yy}^{h} are normal stresses parallel and perpendicular to the fracture surfaces, respectively.

Figure 3 shows the distributions of σ_{xx}^{h} along the perpendicular bisector of the main fracture corresponding to different times of fracture cooling. It is found that at the early times, a large tensile stress component σ_{xx}^{h} can only concentrate very close to the fracture surfaces, and its magnitude far away from the main fracture surface is still very small. However, with the increase of the cooling time, large σ_{xx}^{h} will move into the deep place of the geothermal reservoir. For example, σ_{xx}^{h}=32 MPa at the place of Y=40 m when the cooling time is 10^{9} sec ($\approx$31 years), where Y is the distance from the main fracture surface. These results indicate that the propagation of the secondary thermal fractures may be very slow; however, it is possible for them to deeply penetrate into the reservoir under appropriate conditions.

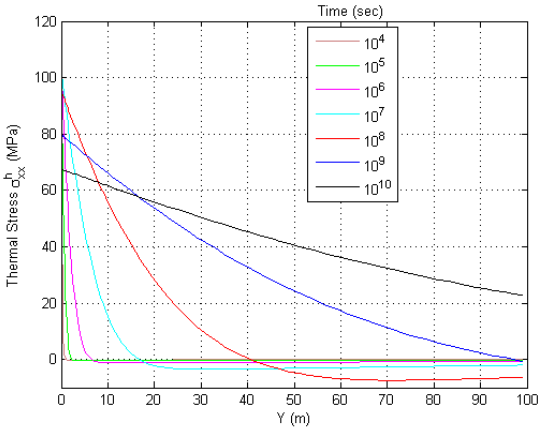

Figure 3. Distributions of the thermally induced normal stress σ_{xx}^{h} corresponding to different cooling times of the main fracture, where Y denotes the distance from the fracture surface.

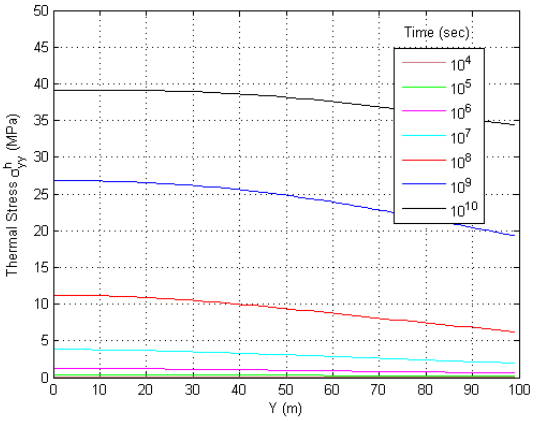

Figure 4. Distributions of the thermally induced normal stress parallel to the fracture surface σ_{yy}^{h} corresponding to different cooling times of the main fracture, where Y denotes the distance from the fracture surface.

Figure 4 shows the distributions of σ_{yy}^{h} along the perpendicular bisector of the main fracture corresponding to different cooling times. It is found that σ_{yy}^{h} is relatively uniform in the direction perpendicular to the main fracture. Its magnitude is initially very small, and increases slowly to about 40

MPa when the cooling time is 10^9 sec ($\approx$31 years). The large magnitude of σ_{yy}^h after the long cooling time would tend to increase the aperture of the main fracture, and may induce new fractures in geothermal reservoirs.

SINGLE SECONDARY THERMAL FRACTURE PROPAGATION

In the previous section, we have shown the potential for the occurrence of large magnitude thermally induced tensile stresses in a geothermal reservoir. In this section, we simulate the propagation of a single secondary thermal fracture. In the real geothermal reservoirs, the fluid may flow into secondary thermal fractures once they are formed and hence, the heat exchange also occurs along secondary thermal fractures. However, considering the fluid flow pattern in the main fracture-secondary thermal fracture system, it can be imagine that the heat exchange through the secondary thermal fractures may not be as efficient as through the main hydraulic fracture. Therefore, here we consider two extreme situations in our simulations: one is that the surfaces of the newly developed secondary thermal fractures are also maintained at the temperature of the main fracture; the other is that the secondary thermal fractures are not cooled. Another factor we need to consider in the simulation is the influence of the in-situ stresses on the development of the secondary thermal fractures.

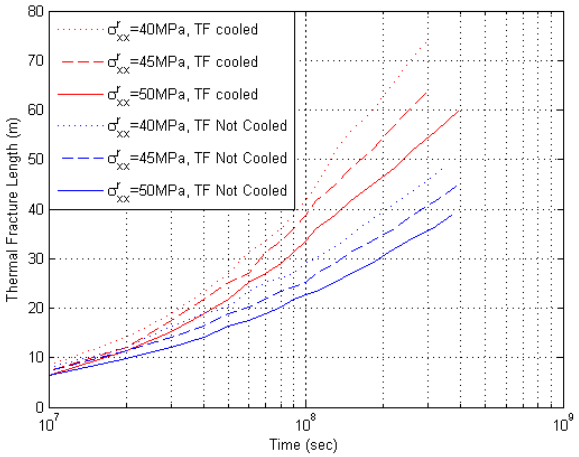

Figure 5. The propagation lengths of a single secondary thermal fracture corresponding to various situations, where σ_{xx}^r is the in-situ normal stress in the x direction.

Figure 5 show the variations of the propagation depth of a single thermal fracture with time, in which the maximum horizontal in-situ stress σ_{xx}^r has assigned values as 40 MPa, 45 MPa, and 50 MPa, while the minimum horizontal in-situ stress σ_{yy}^r is fixed at 40 MPa. Both cooled and uncooled secondary thermal fractures are considered. The results show that the cooling of the secondary thermal fracture can significantly enhance its propagation depth. At the time of 2×10^8 sec (about 6.2 years), the cooled secondary thermal fracture propagates about 1/3 longer than the uncooled ones. We also found that the magnitude of σ_{xx}^r affects the propagation of the secondary thermal fracture, that is the larger the magnitude of σ_{xx}^r, the shorter of the secondary thermal fractures. These results indicate that the secondary thermal fractures may not be able to propagate far away from the main hydraulic fractures in deep geothermal reservoirs where the in-situ stresses are expected to be relatively large.

MULTIPLE SECONDARY THERMAL FRACTURE PROPAGATION

We have shown that a single secondary thermal fracture is able to propagate deeply into the geothermal reservoir under suitable conditions. Having estimated the driving stresses and the penetration of the secondary thermal fractures, it is desirable to estimate the spacing of these secondary thermal fractures. It is well known that fracture propagation is strongly influenced by the mechanical interaction between neighboring fractures throughout the fracture growth history (Segall and Pollard, 1983; Pollard and Aydin, 1988). This interaction is manifested by the opening or shearing of one fracture perturbing the stress field around other nearby fractures. For the present problem, the fracture mechanical interaction suggests that at early times, the secondary thermal fractures will be closely spaced and of very shallow penetration, but with the elapse of the time, fewer but deeper penetration secondary thermal fractures will form (see Figure 1).

The propagations of a three secondary thermal fracture system are simulated, in which all the secondary thermal fractures are not cooled. The parameter and data set used here are shown in Table 1. Figure 6 shows the fracture propagations at the time of about 12 years, in which the temperature difference between the main fracture surface and the initial geothermal reservoir is ΔT =200 K. The location of the main hydraulic fracture in the plots is along the *x* axis. The initial spacing of the secondary thermal fractures is assumed to be 15 m and 25 m, respectively. It is found that at the assigned time, for both of the situations, the growth of the middle one has stopped while the other two are able to continue to grow. This phenomenon is caused by the mechanical interaction of the neighboring fractures, and it is indicated that the minimum spacing at this

length of the secondary thermal fractures should exceed 25 m. Figure 7 shows the same simulation results except that the temperature difference between the main fracture surface and the initial geothermal reservoir is ΔT =300 K. It is found when the initial spacing is 15 m, the middle secondary thermal fracture has stopped; however, when the initial spacing is 25 m, all three secondary thermal fractures can continue to grow. It is implied that for the current length of the secondary thermal fractures, the minimum spacing can be less than 25 m.

(a)

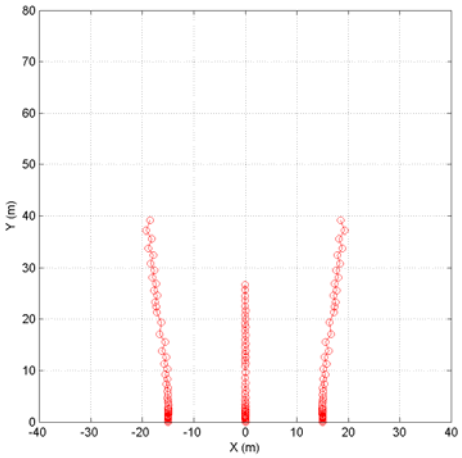

(b)

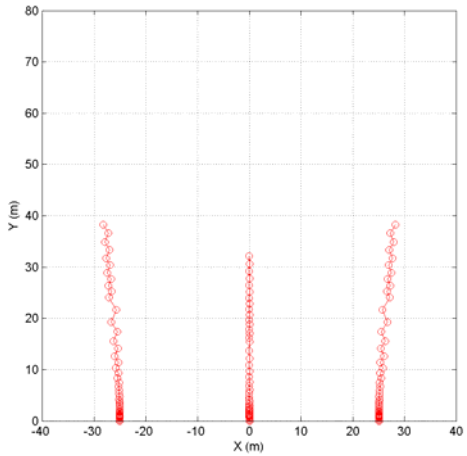

Figure 6. Propagations of three secondary thermal fractures respectively with spacing (a) 15 m and (b) 25 m, in which the temperature difference between the fracture surface and the initial reservoir is 200 K.

The rock cooling rate is equivalent to the cooling temperature applied at the main hydraulic fracture surfaces in the present model, and also equivalent to the fluid injection rate in the real geothermal operation. From these simulation results, we find that the faster cooling rate produces smaller spacing of the secondary thermal fractures, which is consistent with the conclusion for naturally formed columnar joints in cooling volcanic rocks (Degraff and Aydin, 1993).

(a)

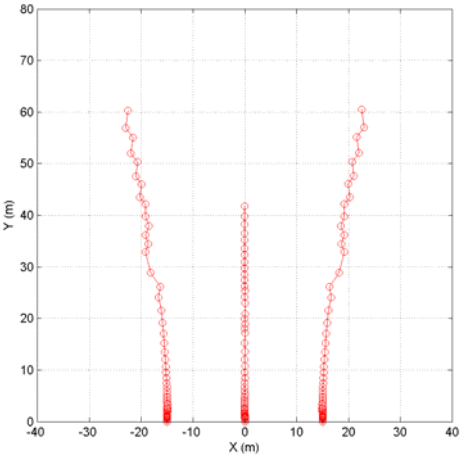

(b)

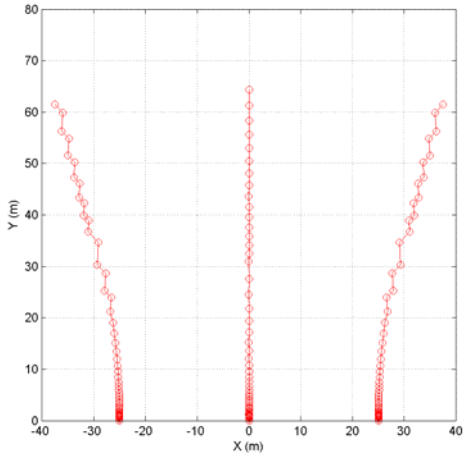

Figure 7. Propagations of three secondary thermal fractures respectively with spacing (a) 15 m and (b) 25 m, in which the temperature difference between the fracture surface and the initial reservoir is 300 K.

In the above analysis, we only studied the spacing of the secondary thermal fractures that are not cooled. If the secondary thermal fractures are also cooled by the secondary circulation of the reservoir fluids, the problem would be more complex, as there are both mechanical and thermal interactions between neighboring secondary thermal fractures. Efforts on these directions are ongoing and will be reported in the future.

SUMMARY AND CONCLUSIONS

We have studied the initiation, propagation, and interaction of secondary thermal fractures due to the cooling of a main hydraulic fracture by reservoir fluids circulation. The thermally induced stresses are

numerically solved by using an integral equation method. The displacement discontinuity method combined with the linear elastic fracture mechanics is used to simulate the secondary thermal fracture propagation, in which the transient thermal stresses are used. The numerical simulation showed that the secondary thermal fractures are able to penetrate deeply into the walls of the main hydraulic fractures under suitable conditions, such as relatively small in-situ stresses and relatively large temperature differences between the fracture surface and the geothermal reservoir. The interaction of the secondary thermal fractures showed that faster cooling rate produces smaller secondary thermal fracture spacing and that length and spacing of the secondary fractures vary as the system evolves from the cooling surface to the interior of the fracture walls.

REFERENCES

Aydin, A. and J.M. Degraff (1993). Effect of thermal regime of growth increment and spacing of contraction joints in Basaltic lava. Journal of Geophysical Research, v. 98, 6411-6430.

Barr, D.T. (1980). Thermal cracking in nonporous geothermal reservoirs. Master thesis, Department of Mechanical Engineering, MIT.

Banerjee, P.K. (1994). The boundary element methods in engineering (2nd ed.). McGraw-Hill: New York.

Cheng A.H.-D. and E. Detournay (1998). On singular integral equations and fundamental solutions of poroelasticity. International Journal of Solids and Structures, v. 35(35), 4521-4555.

Cheng A.H.-D., A. Ghassemi, and E. Detournay (2001). A two-dimensional solution for heat extraction from a fracture in hot dry rock. International Journal for Numerical and Analytical Methods in Geomechanics, v. 25, 1327-1338.

Crouch, S.L. and A.M. Starfield (1983). Boundary Element Methods in Solid Mechanics, ALLEN & UNWIN, INC.

Drdogan, F. and G.C. Sih (1963). On the crack extension in plates under plane loading and transverse shear. Journal of Basic Engineering, December, 519-527.

Hayashi, K., J. Willis-Richards, R.J. Hopkirk, and Y. Niibori (1995). Numerical models of HDR geothermal reservoirs – a review of current thinking and progress. Geothermics, v. 28, 507-518.

Jaeger, J., N.G. Cook, and R. Zimmerman (2007). Fundamentals of Rock Mechanics (4th ed.). Blackwell Publishing.

Mutlu, O. and D.D. Pollard (2008). On the patterns of wing cracks along an outcrop scale flaw: a numerical modeling approach using complementarity. Journal of Geophysical Research, v. 113, B06403, doi:10.1029/2007 JB005284.

Olson, J.E. and D.D. Pollard (1991). The initiation and growth of en-chelon veins. Journal of Structural Geology, v. 13(5), 595-608.

Pollard, D.D. and A. Aydin (1988). Progress in understanding jointing over the past century. Geological Society of America Bulletin, v. 100, 1181-1204.

Segall, P. and D.D. Pollard (1983). Joint formation in granitic rock of the Sierra Nevada. Geological Society of America Bulletin, v. 94, 563-575.

Tester, J.W., H.D. Murphy, C.O. Grigsby, R.M. Potter, and B.A. Robinson (1989). Fractured geothermal reservoir growth induced by heat extraction, SPE Reservoir Engineering, v. 4, 97-104.

Zhou, X.X., A. Ghassemi, and A.H.-D. Cheng (2009). A three-dimensional integral equation model for calculating poro- and thermoelastic stresses induced by cold water injection into a geothermal reservoir. International Journal for Numerical and Analytical Methods in Geomechanics, v. 33(14), 1613-1640.